https://doi.org/10.1016/j.jobe.2018.10.029

Influence of insulation defects on the thermal performance of walls. An experimental and numerical investigation

Iole Nardi, Stefano Perilli, Tullio de Rubeis, Stefano Sfarra, Dario Ambrosini*

Department of Industrial and Information Engineering and Economics, University of L'Aquila,
Piazzale E. Pontieri 1, Monteluco di Roio, L'Aquila, AQ I-67100, Italy

* Corresponding author. Email address: dario.ambrosini@univaq.it; Web: laser.diiie.univaq.it

Abstract: The addition of insulating layers on vertical walls of buildings is a common practice for providing a higher thermal insulation of the envelope. Workmanship defects, however, might influence the effectiveness of such insulation strategy. Damaged materials, incorrect installation, use of aged or weathered materials might alter the capability of reducing heat transfer through the envelope, whether vertical or sloped. In this work, drawbacks caused by the wrong installation of insulating material and by damaged material are assessed. A specimen wall was investigated by experimental and numerical approaches, the latter carried out by using COMSOL Multiphysics®. Results are compared and discussed.

Keyword: Numerical simulation; Heat transfer; Insulating panel; EPS; COMSOL Multiphysics®; Guarded Hot Box

Declarations of interest: none

1. Introduction

High energy consumptions in the building sector (about 32% of total global final energy use), addressed for a share of 34% to space heating [1], are pushing research activities in finding the best solution to avoid, shift and reduce heat waves or losses [2-6].

A key role in this scenario is played by the renovation and refurbishment of the built environment [7, 8]. Such interventions represent the main opportunity of energy efficiency for urban context that, due to energy policies or to reasons of *force majeure*, face the challenge of building renovation. The latter is the case of the city of L'Aquila, in central Italy, that in 2009 was hit by a violent earthquake; most of buildings (both private and public) has undergone (or is still undergoing) reconstruction or renovation [9, 10]. The natural disaster, therefore, has given the opportunity to intervene on several buildings and to improve the energy efficiency. In this sense, the most rapid and common adopted strategy is the addition of insulating layer (the so called ETICS that stands for External Thermal Insulation Composite System). The effectiveness of this solution depends not only on the quality of employed materials, but also on how workmen laid the materials. Each error, damage or omission that occurs during the construction phase might increase the energy performance gap, that is, the difference between predicted and measured energy performance.

Several works deal with defects taxonomy, aiming at providing a definition of "defects" and a possible classification, the phase of occurrence (project, construction or management phase), their major causes and the influences on building thermal performance [11-14]. Several kinds of defects are accounted [13], like detachments, incorrect installation, discontinuities, gaps and thermal bridging. Incorrect installation is one of the most frequent workmanship defects [14]. Obviously, defects can worsen the capabilities and features of the assets on which occur, and quality defects (like those mentioned before) can impact buildings thermal performance, causing local increase of thermal losses, and leading to higher energy consumption

An aid for a better evaluation of building features is provided by software and tools [15-17]. The possibility of investigating building elements by using simulation and computer tools is widening the study of new materials and solutions for the realization or renovation of the built environment. In this sense, calculation codes can reproduce or simulate building elements energy performances, thus they allow to infer the thermal response of elements under different conditions.

Several simulation tools are available, both open source and commercial. Amongst these, COMSOL Multiphysics® is spreading. It is a software platform based on advanced numerical methods that allows the modeling and simulation of physical problems [18].

As shown in recent literature, COMSOL Multiphysics® can be employed for studying several and different building related problems [19-25]; numerical result can be validated by comparison with various control systems such as thermo-flowmeters, thermocouples (as in the case under analysis), and thermographic techniques [26].

However, none of the works available in literature, at the best of authors' knowledge, deals with the employment of COMSOL Multiphysics® for the modeling of the effects of workmanship defects during the installation of materials in buildings, although the issue is quite important.

This paper aims to understand how relevant workmanship defects can be on wall thermal performance.

2. Materials and methods

In this paper, the effects on the temperature field caused by defects in insulating panels were assessed both via COMSOL Multiphysics® and via experimental measuring campaigns.

Two expanded polystyrene (EPS) panels were mounted on a specimen wall: a defective and a flawless one. Tests have been carried out in a controlled environment (*i.e.* a hot box). Heat flow and temperatures were measured on defects and on the flawless panel. A numerical model was then realized by COMSOL Multiphysics®. Numerical results were, then, validated by comparison with superficial temperatures measured, becoming a helpful tool to quantify possible heat losses on buildings.

The paper is structured as follows: section 2 describes the employed methods (the experimental measurements set up, its numerical model, together with the physics of the numerical simulation and the solver mesh). Section 3 reports experimental and numerical data. Section 4, devoted to conclusions, completes the paper.

In this section, the set up employed for experimental campaign is described, together with the numerical model, its governing equations and mesh spacing used for comparison. The assessment procedure of defects effects that relies on the coupling between laboratory data and numerical modeling is shown in Figure 1.

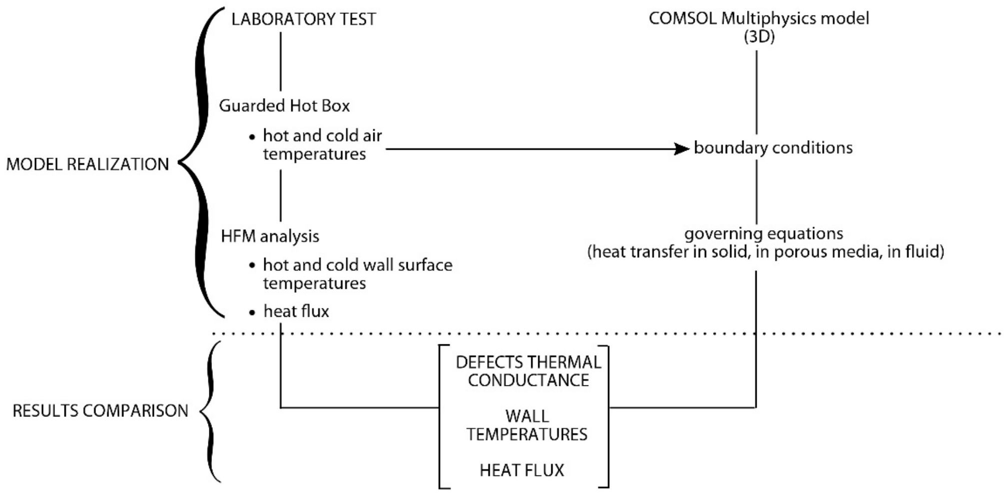

Figure 1. Adopted procedure.

2.1 Test setup

This paper presents the numerical model, built with COMSOL Multiphysics®, of heat transfer through defective and flawless insulation employed as ETICS. The model replicates the realized experimental setup. For the purpose, two EPS panels, whose sizes are 48 cm x 198 cm x 8 cm (LxHxW), were employed: a flawless panel (FP of Figure 2), and a defective one (DP of Figure 2). To replicate a discontinuity of insulation layer, a small piece of the adjacent side of the panels was left without adhesive.

For choosing the defect dimensions, the following considerations were taken into account:

- A defect should be large enough to allow the placing of the flux plate and of the temperature probe in its proximity;
- A defect should be as far as possible from discontinuities since they can cause side effects;
- Defects should not interfere with each other.

Therefore, following a symmetric criterion, the experimental setup shown in Figure 2 was realized. P1 indicates the bonding defect; P2 is a void in the panels, that is, a piece of panel partially hollowed, replicating what occurs for sheaths and wires passage. Sizes of defect P2 are 5 cm x 30 cm x 3 cm (LxHxW), and its layout is show in section A-A'. Point P3 represents a sound area on the flawless panel.

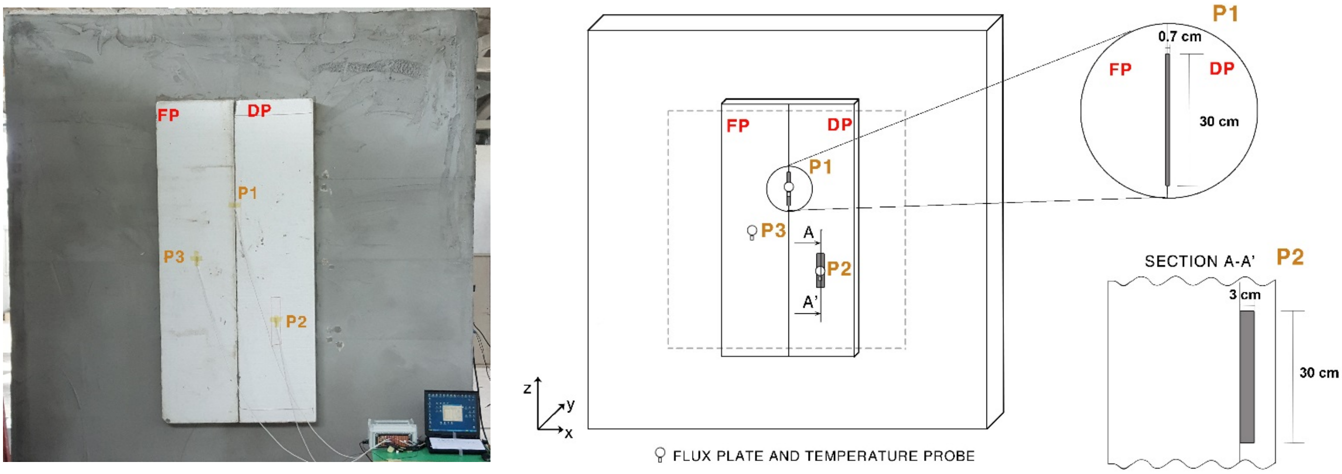

a) b)

Figure 2. Setup and defects details: a) picture; b) drawing with sizes.

The defects length was chosen starting from the assumption proposed in a recent work [12] dealing with insulation defect. In [12], monolayer specimens, whose dimensions were 30 cm x 30 cm, were tested by using a hot plate device, and five defect typologies were investigated, assessing their thermal conductance also according to various aspect ratios. The set up was conceived to reduce edge effects on such small samples.

In our tests, the experimental setup is based on samples of insulating layers, applied on a wall large enough to reproduce real condition of heat losses that might occur on a building.

To guarantee accurate results, a controlled environment was chosen. Therefore, tests were performed in a guarded hot box (GHB).

Panels were glued on the specimen wall of a hot box: the final assembly is shown in Figure 3, together with materials thickness (d) [m] and thermal conductivity (k) [W/(m·K)].

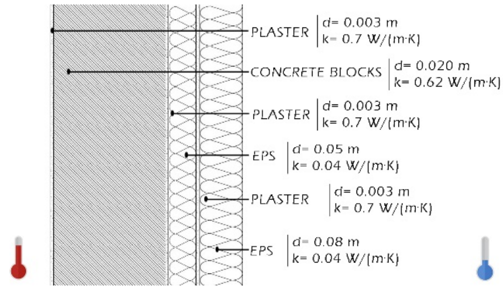

Figure 3. Wall assembly, showing materials thickness (d) and thermal conductivity (k).

As operating principle, a hot box consists of two chambers whose temperatures can be set by acting on a cooling and a heating system (for the cold and hot side, respectively), while the wall under investigation is interposed between the chambers. This system allows setting, on the boundaries of the specimen wall, the desired temperatures.

In this test, a guarded hot box was employed (Figure 4). It is equipped with a cold chamber (CC) and a hot chamber; the latter is composed by a smaller chamber, called metering box (MB) [27, 28], that allows to better confine heat and to prevent two- or three- dimensional heat losses in the wall center. Thus, there is a guard box (GB) that surrounds the metering box.

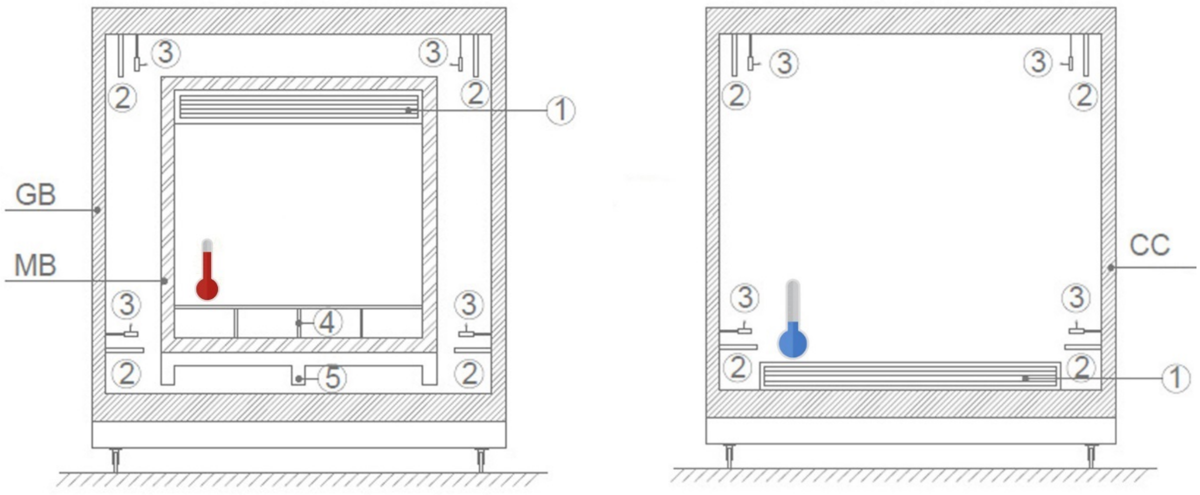

a) b)

CC: cold chamber (sizes: 300 cm x 300 cm) – galvanized steel sheets (0.1 cm) separated by a layer of expanded polyurethane (10 cm)

GB: guard box (sizes: 300 cm x 300 cm) – galvanized steel sheets (0.1 cm) separated by a layer of expanded polyurethane (10 cm)

MB: metering box (sizes: 180 cm x 180 cm) – galvanized steel sheets (0.1 cm) separated by a layer of expanded polyurethane (10 cm)

1: grid fans

2: electric resistances

3: fans

4: metering box support

5: metering box railing

Figure 4. Drawing of the hot box, with sizes and equipment: a) cold chamber; b) hot chamber.

Measurements were carried by clamping the hot chamber to the wall, and by leaving the other side facing the facility that hosts the hot box that, in this way, acts as a cold chamber. The laboratory has an air handling unit to control its temperature.

Regarding the test, three heat flow meters were installed, one for each defect plus one for the flawless panel. Therefore, a flux plate and two temperature probes were mounted for each point of Figure 2.

Flux plates were placed after applying a thin layer of thermal compound, to enhance heat.

Pairs of temperature probes (Pt100 type) were mounted for each point, on the hot and cold wall face, one in correspondence to the other. Moreover, probes on the hot side were placed in proximity of the flux plates. A data set consisting of heat flow rate, wall temperature on the hot and cold side, air temperature of the hot chamber and of the facility was recorded every 10 min and stored by a DeltaT DL2 logger. The measurement campaign lasted 72 hours. This duration was chosen following on one hand the requirement of ISO 9869 [29], that suggests a lasting that is an integer multiple of 24 hours, and on the other hand indication from standard ISO 8990 [30], that does not provide a minimum lasting for measurement via hot boxes, but gives an example criterion for the definition of the steady-state condition.

Following the remarks given in [29], and considering that measurement campaigns are taken under controlled conditions (Hot Box in a laboratory), errors in temperature measurements are assumed within 5% and errors in conductance measurements are assumed about 15%.

2.2 Description of the numerical model

The numerical model describes a wall, as shown in Figure 3. The back of the wall (indicated by a red thermometer in Figure 3) was placed in contact with the hot-side surface of the hot box. In the numerical model, this was represented by a volume, consisting of an air fluid and reproducing the geometry of the chamber. This choice was needed to avoid the imposition of a surface temperature on the wall in a direct way. By directly assigning a surface temperature boundary condition, the model would be numerically forced. To obtain a behavior like the real case, a virtual box (consisting of air) with a thickness of 500 mm was dimensioned.

The temperature boundary condition was imposed on the contour surface of the air box placed opposite to the interface with the analyzed wall. About the contact conditions between the virtual air box and the supporting structure, continuity conditions for the temperature field have been assigned. For the remaining four contour surfaces representing the thickness of the air box, the condition $-n\cdot(-k\nabla T)$ was assigned to avoid the constraint of the temperature in the area proximal to the wall.

In contact with the concrete structure, the polystyrene panels have been reported. The interface between the latter and the structural part has been modeled using a layer of glue.

A splitting area has been represented; it was conceived as an imperfection of contact with respect to the thickness of the polystyrene panels, assuming the lack of adhesive as an inclusion of air. The latter was realized through a cavity having a rectangular section. Furthermore, in the right-hand panel an additional cavity has been created (as indicated in Figure 2, by P2) which also defines a lack of material. The cold chamber was represented similarly to the hot chamber. The relative boundary conditions were imposed with the same procedure described for the hot chamber. Figure 5 shows the geometry of the model, while Figure 6 represents the elements in relation to the materials being analyzed.

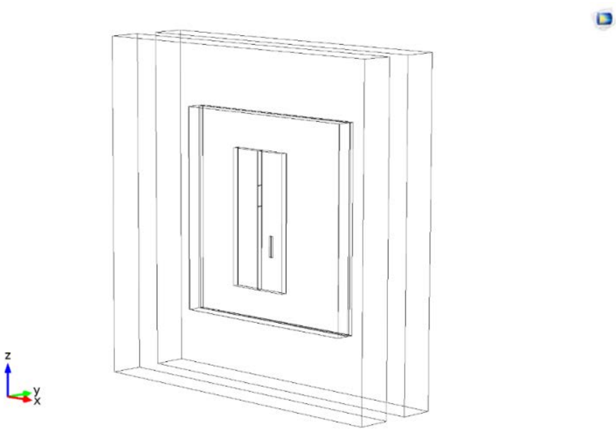

Figure 5. Complete model geometry.

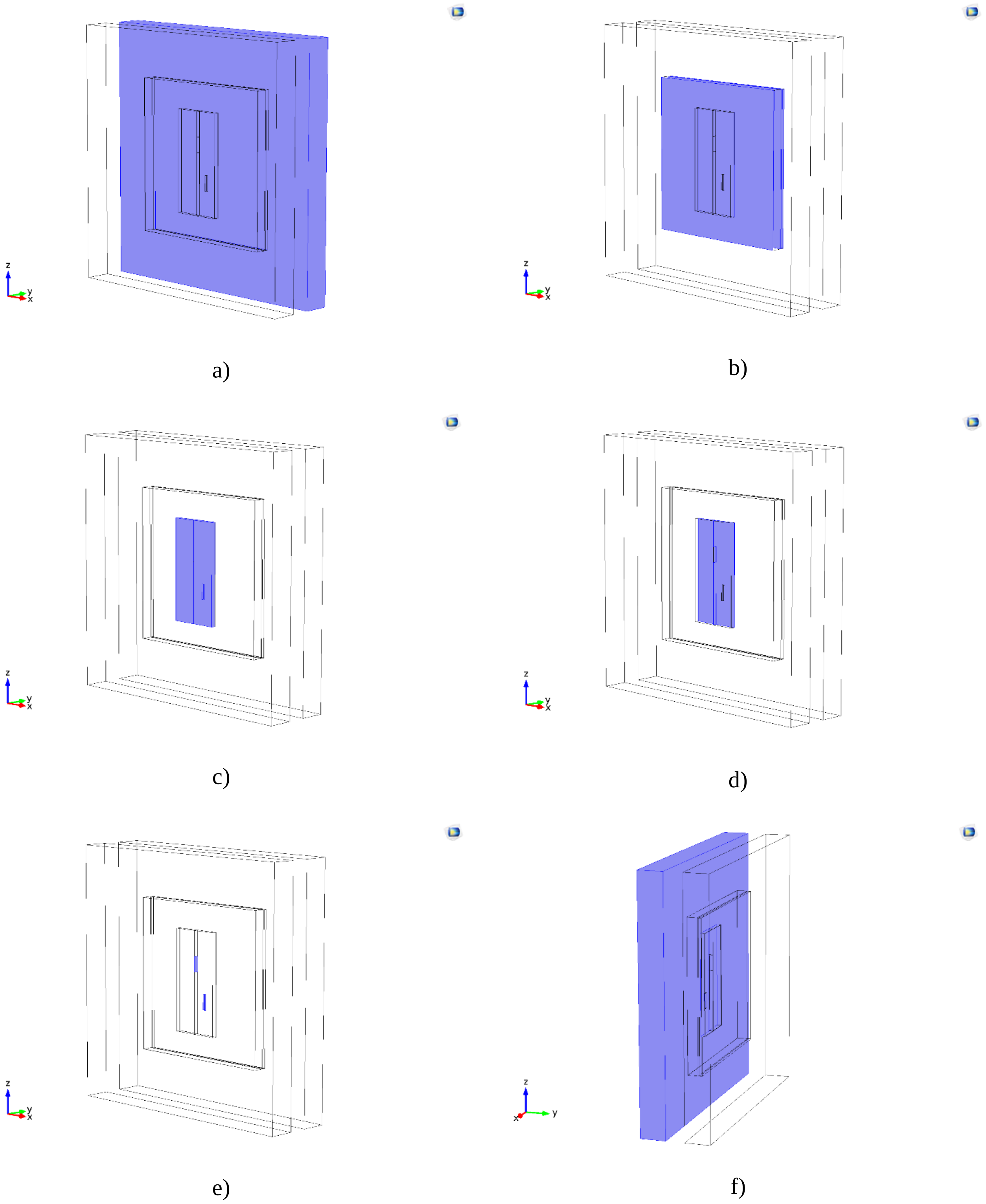

Figure 6. Elements of the model according to the analyzed materials: a) hot chamber (air), b) structural wall, c) polystyrene, d) glue, e) defects (air inclusions), and f) cold chamber.

2.3 Physics of the numerical simulation

The model has a set of governing equations consisting of three mathematical relations: the heat transfer in solid [31] which deals with modeling the elements considered to be free of porosity in the model, the heat transfer in porous media [32] and, finally, the heat transfer in fluids [33] which develops the temperature field in the air fluid.

The first relation is represented by the following equation:

$$\rho C_P \frac{\partial T}{\partial t} + \rho C_P \mathbf{u} \cdot \nabla \mathrm{T} = \nabla \cdot \left(\underbrace{\bar{k} \nabla \mathrm{T}}_{-\mathbf{q}} \right) + Q \tag{1}$$

in which q is the heat flux vector field, i.e., the Fourier's law of heat conduction. Eq. 1 characterizes the behavior of the components shown in Figure 6b. The mathematical equations related to porous elements are:

$$(\rho C_P)_{\mathrm{eff}} \frac{\partial T}{\partial t} + \rho C_P \mathbf{u} \cdot \nabla \mathrm{T} = \nabla \cdot \left(\overline{k_{\mathrm{eff}}} \nabla \mathrm{T} \right) + Q + Q_{\mathrm{vd}} + Q_{\mathrm{P}} \tag{2}$$

$$\left(\rho C_p\right)_{\mathrm{eff}} = \theta_{\mathrm{P}} \rho_{\mathrm{P}} C_{P,P} + (1 - \theta_{\mathrm{P}}) \rho C_p \tag{3}$$

$$k_{\mathrm{eff}} = \theta_{\mathrm{P}} k_{\mathrm{P}} + (1 - \theta_{\mathrm{P}}) k \tag{4}$$

where, at the porosity of the polystyrene has been linked a Θ_P equal to 0.2 [34, 35]. For the heat transfer in fluids, Eq.2 was used with the density expressed as indicated in Eq. 5:

$$\rho = \frac{p_A}{R_S T} \tag{5}$$

The variables in Eq. 1 -5 are described in Table 1.

Table 1. List of variables.

C	Thermal conductance [W/(m^2·K)]
q	Density of heat flow rate or heat flux [W/m^2]
ρ	Density [kg/m^3]
C_P	Specific heat at constant pressure [J/(kg·K)]
$\bar{k}$	Thermal conductivity tensor [W/(m·K)]
T	Temperature [K]
Q	Heat source [J]
$(\rho C_p)_{eff}$	Effective volumetric heat capacity at constant pressure
$\overline{k_{\mathrm{eff}}}$	Effective thermal conductivity tensor [W/(m·K)]
$C_{P,\,P}$	Specific heat at constant pressure for porous materials [J/(kg·K)]
Θ_P	Volume fraction porous materials
ρ_P	Density porous materials [kg/m^3]
k_P	Thermal conductivity composite materials [W/(m·K)]
Q_{VD}	Heat sources viscous dissipation [W/m^3]
Q_P	Heat sources pressure work [W/m^3]
p_a	Absolute pressure [Pa]
R_S	Specific gas constant [J/(kg·K)]

The terms present in Eq. 5, *i.e.*, p_A [Pa] and R_S, are calculated for the air according to the instantaneous temperature conditions.

2.4 Solver mesh and materials of the numerical simulation

The 3D numerical model required a tetrahedral mesh throughout the structure. After the convergence analysis of the mesh, it was possible to bring the minimum quality limit to a very low value, *i.e.*, 8.89e^{-7}. The number of elements of the domain is equal to 444539. To obtain this result, a scaling was performed along the *X*, *Y* and *Z* directions of the mesh, according to the absolute reference of the model. Table 2 shows the setting indications of the mesh.

Table 2. Mesh of the numerical model.

Parts of model	X - direction scale	Y - direction scale	Z – direction scale	Domain elements
Plaster	0.05	1	0.05	28506
Glue (panel-wall)	0.5	1	0.5	9897
Glue (panel-panel)	0.5	1	0.5	10973
Defect in panel	1	1	1	88
Panel	0.5	1	0.5	73308
Chamber	1	1	1	321767

The convergence analysis was carried out to evaluate the performance of the mesh in terms of optimization of the discretization of D.o.F. (Degrees of Freedom) inherent to the geometry analyzed. A mesh approximates to the best a structure when the D.o.F. (calculated through the nodes) discretize smaller and smaller volumes of the solid of interest. On the contrary, the increase in the number of nodes involves a greater number of corresponding equations and, therefore, a greater computational cost. For this reason, through specific optimization procedures of the number of nodal elements constituting the mesh, it is necessary evaluate the appropriate dimension of the element approximating the volume under analysis. It has been found from the geometrical characteristics of the model analyzed that for a dimension of the mesh elements equal to 70 [mm], it was possible to observe the lowerest D.o.F. and, therefore, a lower computational cost. Figure 7 shows the trend of the D.o.F. evaluated according to the maximum size assumed by the mesh element approximating the real geometry. The x-axis shows the maximum sizes of the element for a range from 30 [mm] to 140 [mm]. The choice of this interval took place after the verification of stability of the calculated solutions satisfying the initial conditions. This, per each dimension of the interval previously explained.

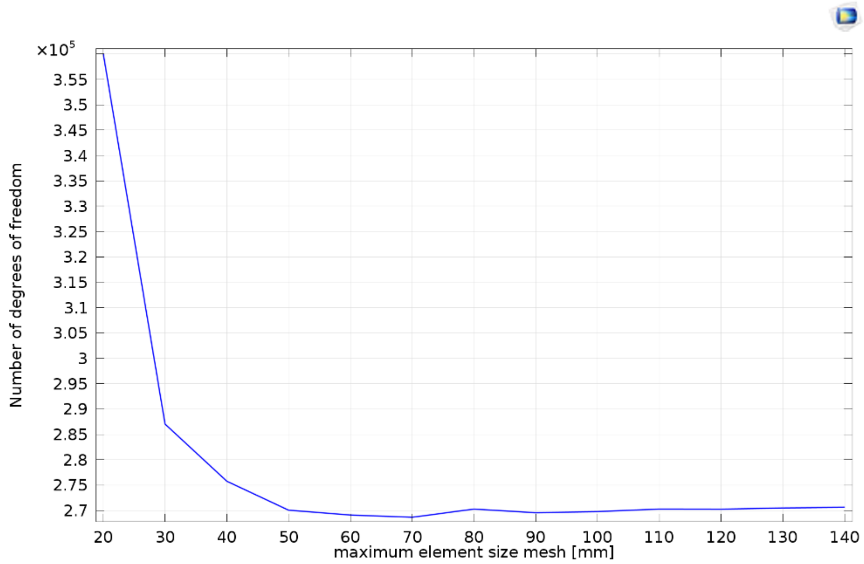

Figure 7. Convergence analysis.

In Figure 8, the mesh of the model is shown.

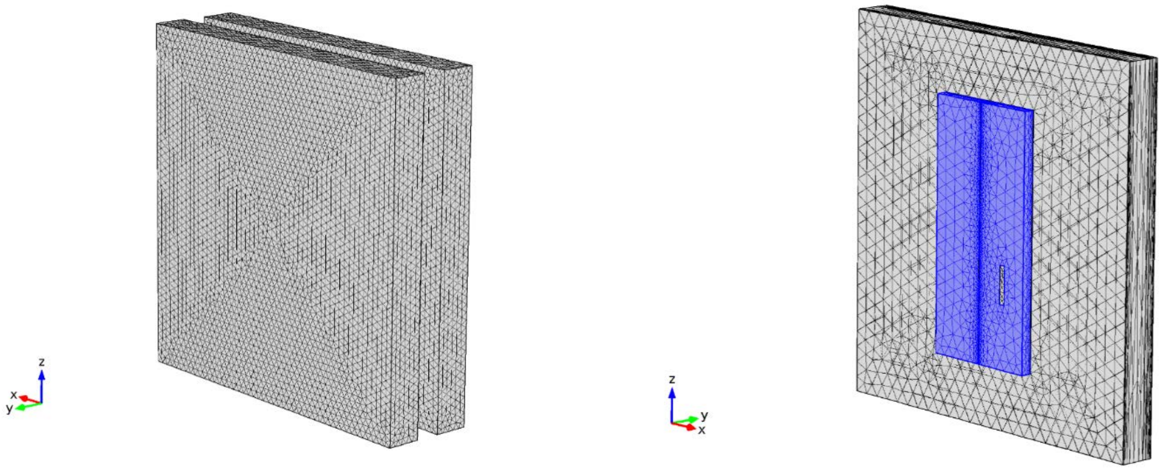

Figure 8. Mesh of the model: a) hot and cold chamber; b) wall with panels and defects.

The model was analyzed with a *fully coupled time dependent solver* for the physics, while a *multigrid* approach was implemented for the geometrical model. The latter was solved with a *Direct* approach.

The selected materials in terms of densities assumed are shown in Table 3.

Table 3. The selected materials and their densities.

Materials	Density $\left[\frac{kg}{m^3}\right]$
Air [36]	1.204
Polystyrene [37]	18
Glue [38]	1700
Concrete [39]	2240
Plaster [40]	802.01

All the other parameters relating to the thermo-physical characteristics are shown in Figure 3 along with the thicknesses.

3 Results

3.1 Experimental data

Data acquired by probes were wall temperature on the hot side $T_{h,w}$ [°C], on the cold side $T_{c,w}$ [°C], and the density of heat flow rate q [W/m^2]. Those data refer to the studied points (namely, P1, P2 and P3), whose location and characteristics are shown in Figure 2. Air temperature in the hot chamber and in the facility that hosted the setup were also recorded, and constituted the input data for the numerical model. Temperature profiles and density of heat flow rate over a 72-h period are shown in Figure 9a and 9b respectively.

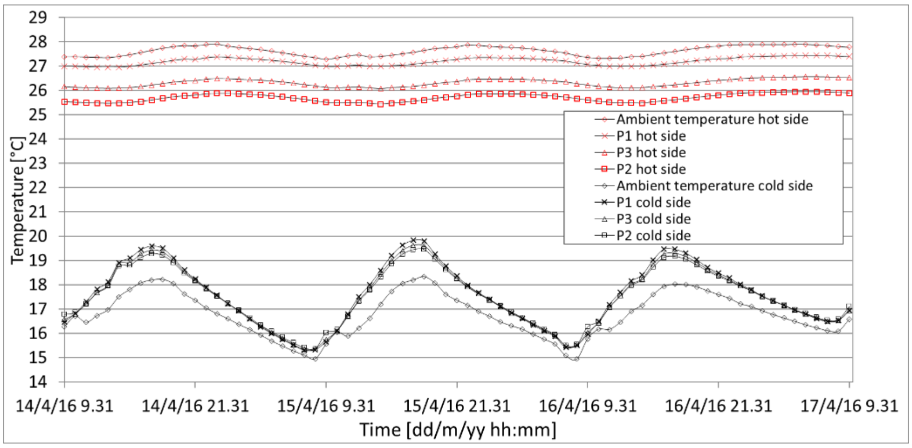

a)

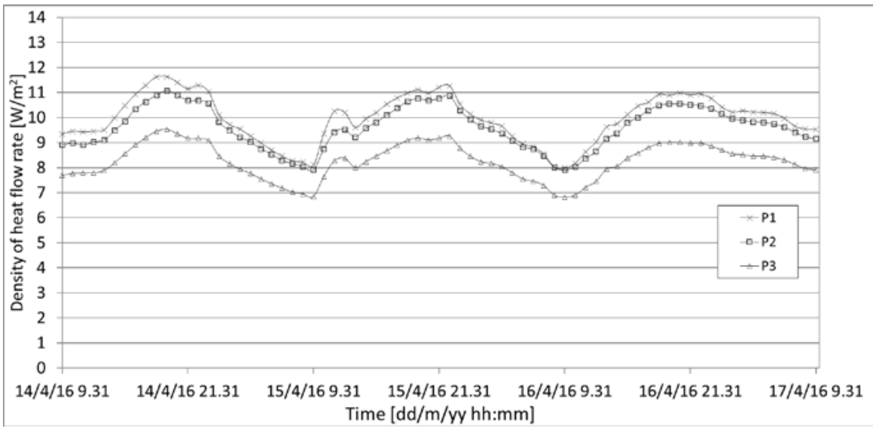

b)

Figure 9. Profiles of instantaneous values of: a) temperatures; b) heat fluxes.

Wall temperatures on the hot side have oscillation with maximum amplitude of 0.5 °C, while air temperature in the hot chamber, that is, the driving force of the heat exchange phenomenon, has an oscillating trend with maximum amplitude of 0.6 °C.

Air on the cold side replicates the outdoor oscillation due to the alternating day/night cycles, and its maximum amplitude is 3.4 °C. Wall temperatures on the cold side have the same oscillating trend, with amplitudes comprise between 4.1 °C (for P2) and 4.5 °C (for P1).

Heat fluxes recorded for the three points are shown in Figure 9b. Trends are similar but appear shifted each other. Heat fluxes on P1 are higher than those on P2 that are higher than those on P3. It is interesting to analyze these results in terms of percentage difference (Figure 10) from P3 that is on a “sound area”. Percentage difference between heat flux on P1 and P3 is quite regular, having a mean value of 20.5%; percentage difference between heat flux on P2 and P3 is more stable, and has a mean value of 16.1%.

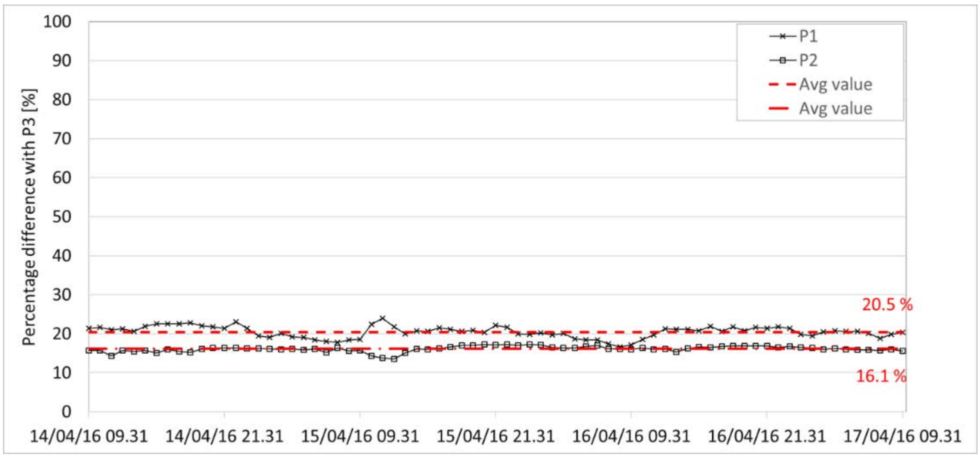

Figure 10. Heat fluxes percentage differences (compared to values on P3).

By employing HFMs, it is possible to evaluate the thermal conductance on measured points for each i^{th} of the n measurements, as the ratio between the heat flux and the difference between superficial temperatures on the hot and cold side, Eq. (6):

$$C_i = \frac{q_i}{T_{h,w,i} - T_{c,w,i}} \tag{6}$$

By applying the average method [29], as per Eq. (7), it is possible to assess the averaged trend of conductances, distinguished in the following by subscripts that refer to the measured points.

$$C = \frac{\sum_{i=1}^{n} q_i}{\sum_{i=1}^{n}(T_{h,w,i} - T_{c,w,i})} \tag{7}$$

Figure 11 and Figure 12 show, respectively, percentage and absolute difference of averaged thermal conductances, compared to values on P3 (sound area). Absolute differences have dumped oscillating trends, with maximum values marked in the Figure.

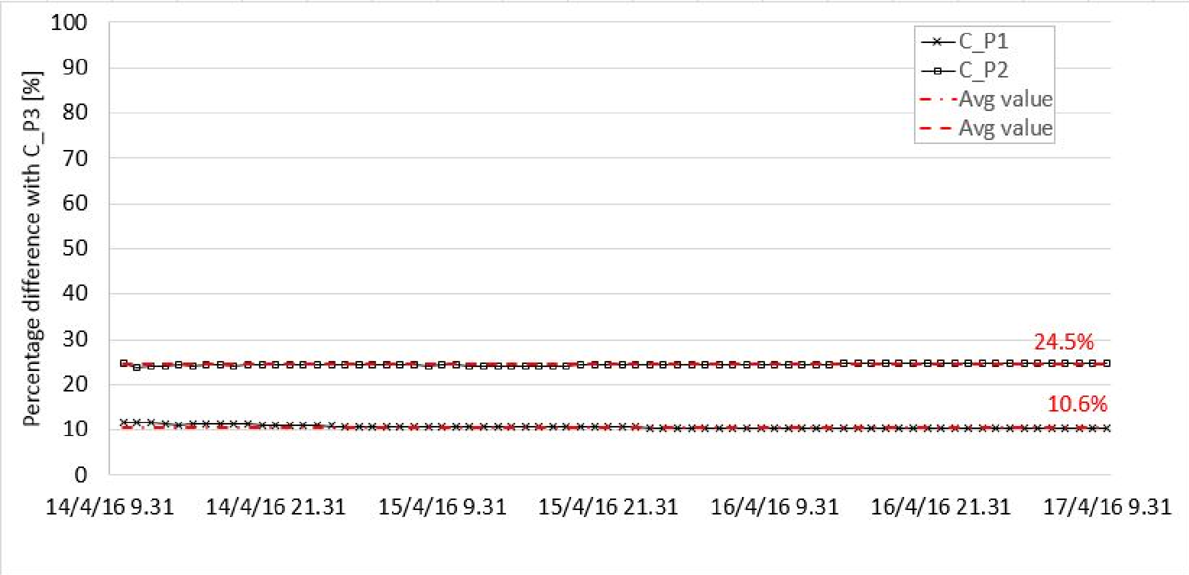

Figure 11. Conductances percentage differences (compared to values on P3).

Figure 12. Conductances absolute differences (compared to values on P3).

Given the results shown in Figure 11 and Figure 12, the defect type that most affects the insulating capability is the void (P2). Nevertheless, defect P1 is more likely to occur on real walls.

3.2 Numerical data

The numerical model shows for the surfaces in contact with the hot chamber and the cold chamber, the virtual probes useful for the control of the wall surface temperatures. In Figure 13, the probes as they appear in COMSOL Multiphysics® are added.

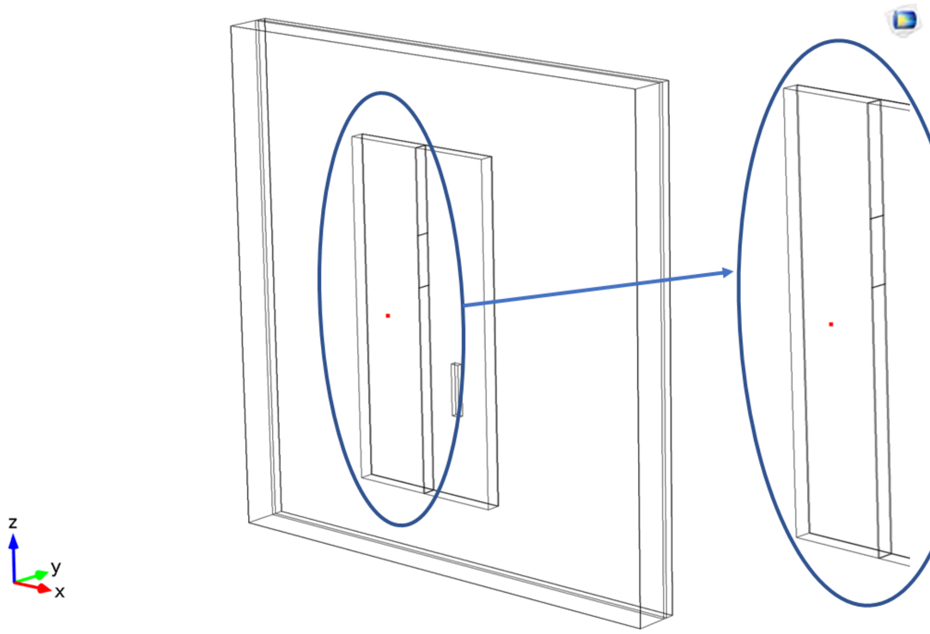

a)

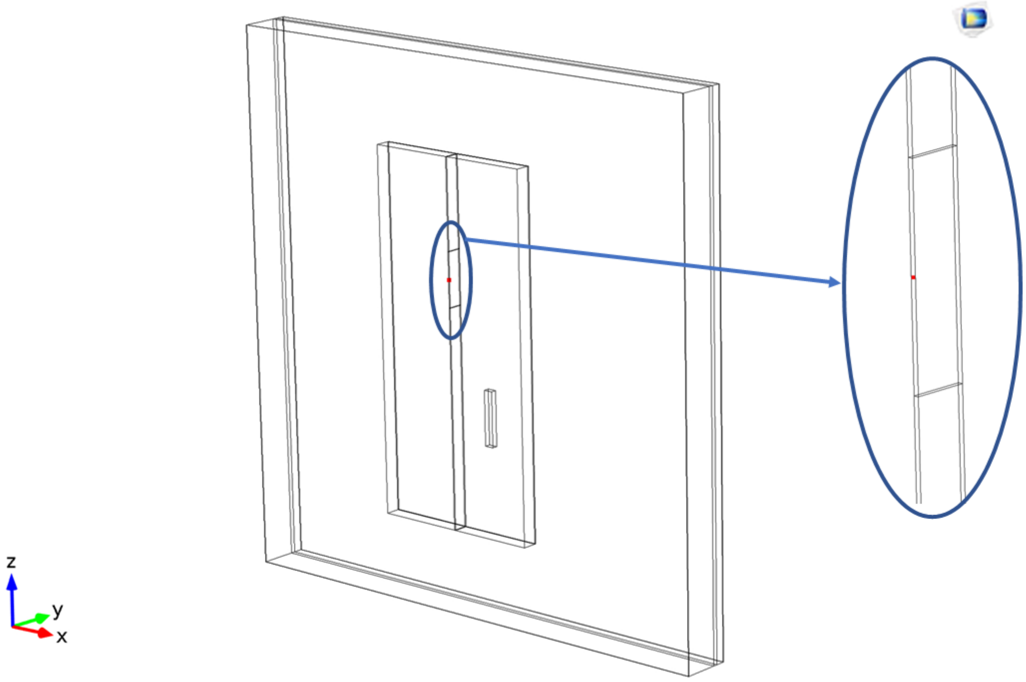

b)

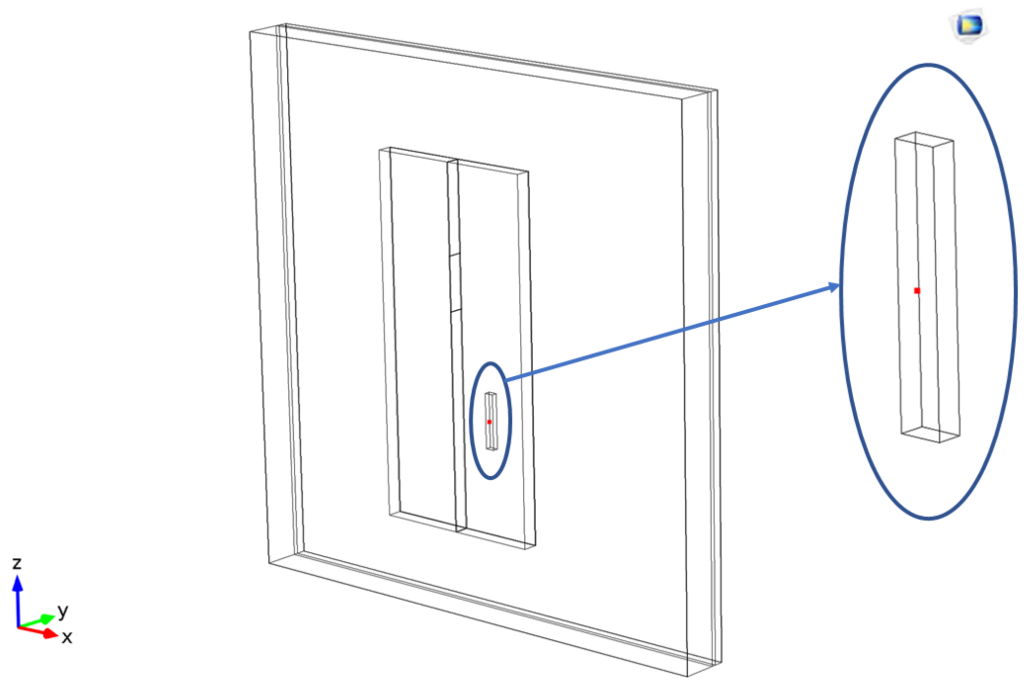

c)

Figure 13. Positions of the virtual probes on the wall surface of the cold chamber: a) center of the polystyrene panel (*P3*), b) center of the defect of gluing (air *P1*), c) center of the “batten” made of air (*P2*).

In Figure 13, only the virtual probes of the cold chamber are reported because concerning the side of the hot chamber, the probes are only translated with respect to the Y axis up to the contact with the foremost plaster surface.

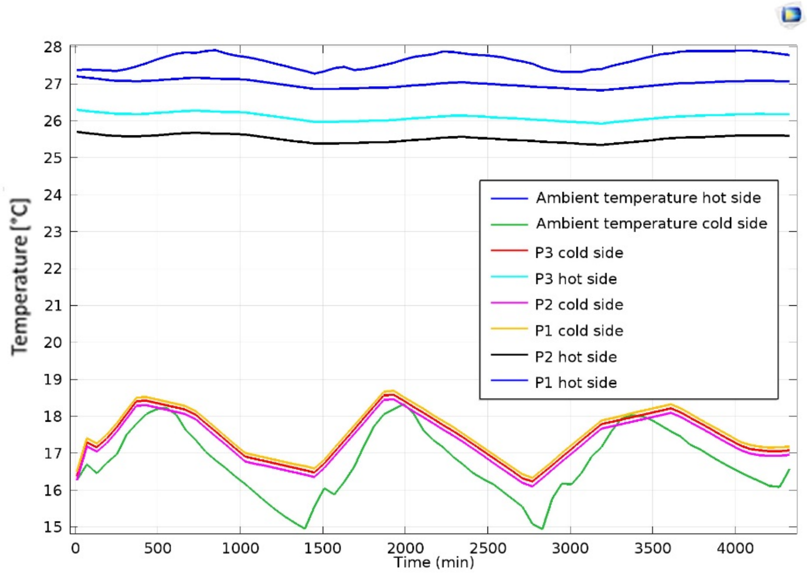

Figure 14. Trend of the surface temperature field for the elements shown in the figure.

In Figure 14, the temperature trends of the virtual probes are shown.

The curve with the highest temperature values in Figure 14 represents the trend of the temperature field of the hot chamber. The input values of the numerical model are exactly coincident with the measured case. This because the temperature profile used in the hot box was set by the authors. For the temperature profile of the cold chamber, the trend highlighted by the curve with the smaller values is obtained. It is coincident with the real case, too.

The remaining curves identify the temperature profile trends coming from the virtual probes, for the surfaces near to both the hot and cold chamber.

The initial values reported by the virtual probes were retrieved thanks to a first calculation step, *i.e.* by evaluating the equilibrium temperature of the system in stationary conditions at the initial instant.

The values obtained per probe from this analysis were used as initial conditions in the final model. By a comparison of the trends of the curves measured in Figure 9a and those simulated in Figure 14, it is possible to see an agreement in the behavior both in terms of oscillation and values. Also, the alternation in the position of the curves indicating P1, P2, and P3 is met. On one hand, the temperature profiles of the probes related to the side of the hot chamber are in perfect agreement with the measured case.

On the other hand, the temperature profiles of the probes installed on the surface in contact with the cold chamber are oscillating with the same period of temperature set for the cold environment. Where the cold chamber has peaks of temperature (at ≈ 600, 2000 and 3400 min), the probe trends intersect the room temperature curve.

In Figure 9a, the intersection between the room temperature and the curves indicating the probe temperatures does not occur. If the model is forced by the boundary conditions, it would not have been possible to verify a crossing between the probe trends and the room temperature curve representing the cold chamber.

Therefore, this proves that the model is free to evolve despite being placed between two environments at assigned temperature.

In Figure 15, the trend of the heat flux evaluated in correspondence with P1, P2 and P3 is shown.

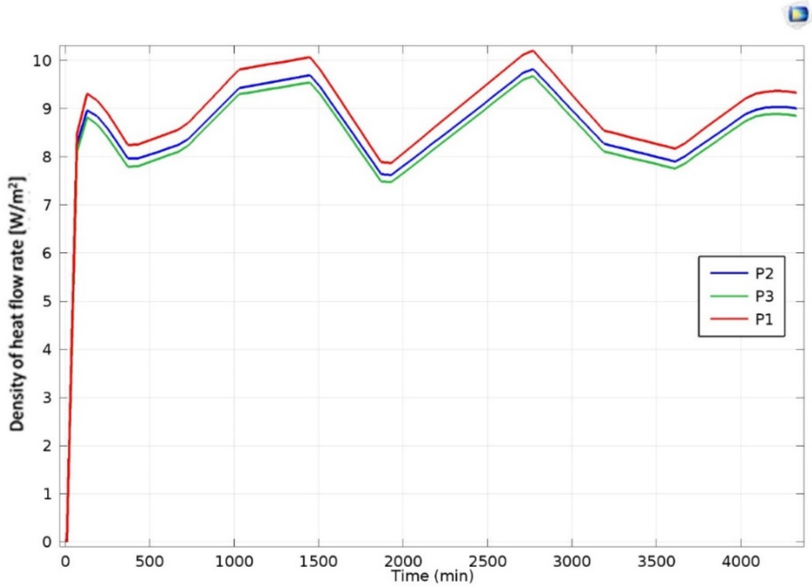

Figure 15. Heat flux trend.

The trend shown in Figure 15 is the simulated heat flux. Comparing the trends with respect to the curve of Figure 9b, the values of the heat flux are of the same order of magnitude. For the simulated case, the maximum peak is ≈ 10.2 [W/m^2] with respect to the peak of the measured value of ≈ 11 [W/m^2]. Unless this difference, the curves for P1, P2 and P3 are in the same sequence but with a slight shift of the oscillation with respect to time.

The starting from zero for the simulated case is typical of the numerical model. At the initial instant of the calculation, the temperature parameters are assigned as boundary conditions; they assume a non-zero value.

No condition was set for the thermal flux; therefore, the system assigned a value equal to zero. Only after the calculation, in the central points of the mesh is linked a value of the heat flux.

From the analysis carried out by COMSOL Multiphysics®, it is possible to see that the model predicts the trends with good agreement with respect to the real case.

3.3 Results comparison

Results from measurements and modeling can differ due to several factors: instrumentation calibration, data acquisition error, boundary condition variation, biased materials characteristics, governing equation, etc. However, to compare and discuss results, in terms of thermal conductance, of simulations (S) and of experimental survey (M), the root mean square error (RMSE), the mean absolute error (MAE) and the mean bias error (MBE) have been employed [41]. Such values have been calculated according to Equations (8-10), where *n* is the number of data, and are shown in Table 4.

$$RMSE = \sqrt{\frac{\sum_1^n (S-M)^2}{n}} \quad (8)$$

$$MAE = \frac{\sum_1^n |S-M|}{n} \quad (9)$$

$$MBE = \frac{\sum_1^n S-M}{n} \quad (10)$$

Table 4. RMSE, MAE and MBE between simulated and experimental values.

	C_P1	C_P2	C_P3
RMSE [W/(m^2K)]	0.17	0.17	0.06
MAE [W/(m^2K)]	0.16	0.15	0.05
MBE [W/(m^2K)]	-0.16	-0.15	0.02

Given the results analysis shown in Table 4, it is possible to infer that there is a good agreement between experimental and numerical results on the flawless point P3, since MBE and MAE are lower than or equal to 0.05 W/(m^2K). There is an acceptable agreement between results of P2 and P1 (panels defects), too; in these cases, differences are of the order of 15-16%.

Conclusions

The frequent recourse to the employment of ETICS for the reduction of building thermal losses implies the need for the evaluation of workmanship defects during its installation. A few works in literature deal with this issue, and none has been carried out of specimen wall. This paper aims at filling this gap, and it deals with the evaluation of the effects of defects on insulating capabilities of EPS panels.

Particularly, workmanship defects have been reproduced on twin panels glued on a specimen wall belonging to a guarded hot box (GHB). The use of a GHB allowed the temperature setting on one side of the wall (hot side), while the other side was kept in contact with the air of the facility that hosts the GHB, equipped with an air handling unit. The set up aims at mimicking what might occur on real wall refurbished with the addition of an external insulating panel in case of panel corruption. Two kinds of defects were reproduced: (i) the lack of continuity of the insulation layer, caused for instance by the absence of adhesive/glue between two adjacent panels (namely, defect P1); (ii) a partial void on panel, caused for instance by sheaths and wires passage (namely, defect P2).

Sizes and location of defects were properly chosen, according to previous literature experiences.

Three reference points (one for each defect plus one on a "sound area"–point P3) were selected for the measuring campaign, based on the heat flow meter method. Therefore, three heat flux plates and six surface temperature probes were installed on the reference points, to evaluate the effects of defects on the thermal conductance of the wall.

Moreover, two probes monitored and logged the air temperature on the hot and cold side of the wall. These data constituted the input (as boundary conditions) of the numerical model developed by the authors using COMSOL Multiphysics®. The model faithfully represents the wall, the panels, and the two defects and, moreover, has virtual probes for the temperature and flux evaluation in correspondence to the reference points. Model's governing equations also consider the porosity of the insulating panels.

Experimental results were compared with the numerical responses gathered by the finite element analysis. The following outcomes can be pointed out from the results:

- Wall temperatures on the hot side have the same oscillating trend of the air temperature, the latter being conditioned by the heating system of the GHB. Temperature of P1 is higher (0.88 °C on average) of that of P3, that differs by 0.62 °C (on average) from that of P2. This implies that the air cavity of P2 lowers the wall temperature on the cold side;

- Wall temperatures on the cold side have the same oscillating trend of the air temperature, the latter being conditioned by the air handling unit of the laboratory. Temperatures of P1, P2 and P3 on the cold side are quite similar, as shown in Figure 9a). This implies that the effects of defects on temperatures on the cold side are smoothened. Moreover, wall temperatures on the cold side seem to differ more when the three peaks are reached;
- By comparing instantaneous values of heat flux measured on the flawless point and on the two defects, it can be pointed out that flux on P1 and on P2 differ on average by 20.5% and 16.1% respectively from flux on P3. That is, the heat flux that crosses the wall with a bonding defect is one-fifth bigger than that crossing the sound area;
- The defect type that much worsens the insulating capability is the void (P2). Nevertheless, defect P1 is more likely to occur on real walls;
- The finite element model proposed fully represents the heat exchange phenomena occurred during the measuring campaign. This is due on one hand on the proper choice of the governing equations, that include the evaluation of materials porosity, on the other hand on the accurate modeling of materials properties, to which the model seemed quite sensitive;
- The initial values reported by the virtual probes were retrieved thanks to a first calculation step. This was needed to evaluate the equilibrium temperature of the system in stationary conditions at the initial instant. The values obtained by using probes from this analysis were used as initial conditions in the final model;
- Comparing measured and modeled temperatures trends, it is possible to see an agreement in the behavior both in terms of oscillation and values. Also, the alternation in the position of the curves indicating P1, P2, and P3 is met;
- The numerical model, with its proper equations, is free to evolve despite being placed between two environments (hot and cold chamber) at assigned temperature.

Acknowledgments

The authors thank Mr. Giovanni Pasqualoni (University of L'Aquila) for the support during the experimental measurements in the "G. Parolini" Laboratory.

Funding:

This research did not receive any specific grant from funding agencies in the public, commercial, or not-for-profit sectors.

References

[1] O. Lucon, D. Ürge-Vorsatz, A. Zain Ahmed, H. Akbari, P. Bertoldi, L. F. Cabeza, N. Eyre, A. Gadgil, L. D. D. Harvey, Y. Jiang, E. Liphoto, S. Mirasgedis, S. Murakami, J. Parikh, C. Pyke, M. V. Vilariño, 2014: Buildings. In: Climate Change 2014: Mitigation of Climate Change. Contribution of Working Group III to the Fifth Assessment Report of the Intergovernmental Panel on Climate Change [Edenhofer, O., R. Pichs-Madruga, Y. Sokona, E. Farahani, S. Kadner, K. Seyboth, A. Adler, I. Baum, S. Brunner, P. Eickemeier, B. Kriemann, J. Savolainen, S. Schlömer, C. von Stechow, T. Zwickel and J.C. Minx (eds.)]. Cambridge University Press, Cambridge, United Kingdom and New York, NY, USA.

[2] Ascione, F., De Masi, R. F., Mastrullo, R. M., Ruggiero, S., Vanoli, G. P. (2017). Experimental investigation and numerical evaluation of adoption of multi- layered wall with vacuum insulation panel for typical Mediterranean climate. Energy and Buildings. http://doi.org/10.1016/j.enbuild.2017.07.029

[3] Mazzeo, D., Oliveti, G., Arcuri, N. (2016). Influence of internal and external boundary conditions on the decrement factor and time lag heat flux of building walls in steady periodic regime. Applied Energy, 164, 509–531. http://doi.org/10.1016/j.apenergy.2015.11.076

[4] Asan, H., Sancaktar, Y. S (1998). Effects of wall 's thermophysical properties on time lag and decrement factor. Energy and Buildings, 28, 159–166. http://doi.org/10.1016/S0378-7788(98)00007-3

[5] Zhang, L. Y., Jin, L. W., Wang, Z. N., Zhang, J. Y., Liu, X., Zhang, L. H. (2015). Effects of wall configuration on building energy performance subject to different climatic zones of China. Applied Energy, 185, 1565–1573. http://doi.org/10.1016/j.apenergy.2015.10.086

[6] Ozel, M. (2014). Effect of insulation location on dynamic heat-transfer characteristics of building external walls and optimization of insulation thickness. Energy and Buildings, 72, 288–295. http://doi.org/10.1016/j.enbuild.2013.11.015

[7] Mazzarella L. (2015) Energy retrofit of historic and existing buildings. the legislative and regulatory point of view. Energy and Buildings, 95, 23-31.

[8] Salvalai G., Sesana M., Iannaccone G. (2017). Deep renovation of multi-storey multi-owner existing residential buildings: a pilot case study in Italy. Energy and Buildings, 148, 23-36.

[9] Nardi I., de Rubeis T., Perilli S. (2016). Ageing effects on the thermal performance of two different well-insulated buildings. Energy Procedia, 101

[10] OpenData Ricostruzione, http://opendataricostruzione.gssi.it/, accessed on April 2018.

[11] Candoré, J. C., Bodnar, J. L., Szeflinski, A., Ibos, L., Datcu, S., Candau, Y., Mattéï, S., Frichet, J.-C. (2008). Helps with the thermal diagnosis of the building: Detection of defects of insulation by stimulated infra-red thermography. Proc. QIRT 2008 - 9th International Conference on Quantitative InfraRed Thermography, July 2-5, 2008, Krakow - Poland.

[12] Aïssani, A., Chateauneuf, A., Fontaine, J.-P., Audebert, P. (2016). Quantification of workmanship insulation defects and their impact on the thermal performance of building facades. Applied Energy, 165, 272–284.

[13] Alencastro, J., Fuertes, A., de Wilde, P. (2018). The relationship between quality defects and the thermal performance of buildings. Renewable and Sustainable Energy Reviews, 81(December 2016), 883–894.

[14] Forcada, N., Macarulla, M., Gangolells, M., Casals, M. (2014). Assessment of construction defects in residential buildings in Spain. Building Research & Information, 42(5), 629–640.

[15] Barreira, E., Delgado, J. M. P. Q., Ramos, N. M. M., de Freitas, V. P. (2013). Exterior condensations on facades: numerical simulation of the undercooling phenomenon. Journal of Building Performance Simulation, 6, 337-345. https://doi.org/10.1080/19401493.2011.560685

[16] Laaroussi, N., Lauriat, G., Raefat, S., Garoum, M., Ahachad, M. (2017). An example of comparison between ISO Norm calculations and full CFD simulations of thermal performances of hollow bricks. Journal of Building Engineering, 11, 69-81. https://doi.org/10.1016/j.jobe.2017.03.011

[17] Jain Megha, Pathak, K. K. (2018). Thermal modelling of insulator for energy saving in existing residential building. Journal of Building Engineering, 19, 62-68. https://doi.org/10.1016/j.jobe.2018.04.012

[18] COMSOL Multiphysics®, https://www.comsol.com/, accessed on April 2018.

[19] Gerlich, V., Oplustil, M., Pisan, R., Zalesak, M. (2012). Benchmark of COMSOL multiphysics via in-depth floor slab test - Transient cases. Energy Procedia, 14, 744–749. http://doi.org/10.1016/j.egypro.2011.12.1005

[20] Perilli, S., Sfarra, Ambrosini, D., Paoletti, D., Mai, S., Scozzafava, M., Yao, Y., (2018), Combined experimental and computational approach for defect detection in precious walls built in indoor environment, International Journal of Thermal Sciences, 129, 29-46. https://doi.org/10.1016/j.ijthermalsci.2018.02.026

[21] Baghban, M. H., Hovde, P. J., Gustavsen, A. (2010). Numerical Simulation of a Building Envelope with High Performance Materials. COMSOL Conference 2010 Paris, 1–5.

[22] Vavilov, V. P., Marinetti, S., Nesteruk, D. A. (2009). Evaluating the thermal resistance of building structures by using infrared thermography under transient conditions. Russian Journal of Nondestructive Testing, 45(7), 481–490. http://doi.org/10.1134/s1061830909070079

[23] Balocco, C., Grazzini, G. (2009). Numerical simulation of ancient natural ventilation systems of historical buildings. A case study in Palermo. Journal of Cultural Heritage, 10(2), 313–318. http://doi.org/10.1016/j.culher.2008.03.008

[24] Asdrubali, F., Pisello, A. L., D'Alessandro, F., Bianchi, F., Fabiani, C., Cornicchia, M., Rotili, A. (2016). Experimental and numerical characterization of innovative cardboard based panels: Thermal and acoustic performance analysis and life cycle assessment. Building and Environment, 95, 145–159. http://doi.org/10.1016/j.buildenv.2015.09.003

[25] Gerlich, V., Sulovská, K., Zálešák, M. (2013). COMSOL Multiphysics validation as simulation software for heat transfer calculation in buildings: Building simulation software validation. Measurement: Journal of the International Measurement Confederation, 46(6), 2003–2012. http://doi.org/10.1016/j.measurement.2013.02.020

[26] Aversa, P., Palumbo, D., Donatelli, A., Tamborrino, R., Ancona, F., Galietti, U., &Luprano, V. A. M. (2017). Infrared thermography for the investigation of dynamic thermal behaviour of opaque building elements: comparison between empty and filled with hemp fibres prototype walls. Energy and Buildings. http://doi.org/10.1016/j.enbuild.2017.07.055

[27] Nardi, I., Ambrosini, D., de Rubeis, T., Sfarra, S., Perilli, S., Pasqualoni, G. (2015). A comparison between thermographic and flow-meter methods for the evaluation of thermal transmittance of different wall constructions. Journal of Physics: Conference Series, 655(1), 12007. http://doi.org/10.1088/1742-6596/655/1/012007

[28] Nardi, I., Paoletti, D., Ambrosini, D., Rubeis, T. De, Sfarra, S. (2016). U -value assessment by infrared thermography: a comparison of different calculation methods in a Guarded Hot Box. Energy & Buildings, 122, 211–221. http://doi.org/10.1016/j.enbuild.2016.04.017

[29] International Standard ISO 9869-1, Thermal insulation. Building elements. In-situ measurement of thermal resistance and thermal transmittance, Part 1: Heat flow meter method, 2014.

[30] European Standard EN ISO 8990, Thermal insulation – Determination of steady-state thermal transmission properties – Calibrated and Guarded Hot Box, 1994.

[31] Bejan A., 1993, Heat Transfer, John Wiley & Sons.

[32] Nield D.A., Bejan A., (2013), Convection in porous media, in: Convection Heat Transfer, 4rd ed., John Wiley & Sons, Inc, Hoboken, N.J., USA.

[33] Batchelor G.K., 2000, An Introduction to Fluid Dynamics, Cambridge University Press.

[34] Cobîrzan N., Balog A.-A., Belean B., Borodi G., Dădârlat D., Streza M. (2016). Thermophysical properties of masonry units: Accurate characterization by means of photothermal techniques and relationship to porosity and mineral composition. Construction and Building Materials, 105, 297–306. http://dx.doi.org/10.1016/j.conbuildmat.2015.12.056

[35] Ochs F., Heidemann W., Müller-Steinhagen H., (2008), Effective thermal conductivity of moistened insulation materials as a function of temperature, International Journal of Heat and Mass Transfer, 51, 539–552. doi:10.1016/j.ijheatmasstransfer.2007.05.005

[36] The Engineering Toolbox, https://www.engineeringtoolbox.com/air-density-specific-weight-d_600.html accessed January 2018.

[37] Fassa Bortolo, http://www.fassabortolo.it/documents/10179/554502/FASSA_STE_IT_LASTRA-ISOLANTE-IN-EPS-100_2016-05.pdf/8d87297f-36ba-459d-8f79-9f7cdd680c11 accessed January 2018.

[38] Mapei, http://www.mapei.com/docs/librariesprovider2/products-documents/361_adesilex_fis13_it239aa07179c562e49128ff01007028e9.pdf?sfvrsn=1aa11df8_0 accessed January 2018.

[39] Harith, I.K., (2018), Study on polyurethane foamed concrete for use in structural applications, Case Studies in Construction Materials, 8, 79-86. https://doi.org/10.1016/j.cscm.2017.11.005

[40] Lamrani, M., Laaroussib, N., Khabbazi, A., Khalfaoui, M., Garoumb, M., Feiz, A., (2017), Experimental study of thermal properties of a new ecological building material based on peanut shells and plaster, Case Studies in Construction Materials, 7, 294-304. https://doi.org/10.1016/j.cscm.2017.09.006

[41] de Rubeis, T.; Nardi, I.; Ambrosini, D.; Paoletti, D. Is a self-sufficient building energy efficient? Lesson learned from a case study in Mediterranean climate. Applied Energy 2018, 218, 131–145, doi:10.1016/j.apenergy.2018.02.166.